Available online at www.sciencedirect.com

ScienceDirect

Procedia CIRP 55 (2016) 109 – 114

www.elsevier.com/locate/procedia

5th CIRP Global Web Conference Research and Innovation for Future Production

Finite element modelling of Wire-Arc-Additive-Manufacturing process

Filippo Montevecchi[a,*], Giuseppe Venturini[a], Antonio Scippa[a], Gianni Campatelli[a]

[a]*Department of Industrial Engineering, University of Firenze, Via di Santa Marta 3, Firenze, 50139, Italy*

* Corresponding author. Tel.: +39-055-2758726. *E-mail address:* filippo.montevecchi@unifi.it

Abstract

Wire-Arc-Additive-Manufacturing (WAAM) is an Additive-Manufacturing (AM) process, allowing to produce metal components layer by layer by means of Gas-Metal-Arc-Welding (GMAW) technology. The advantages of this technology are the capability to create large parts with a higher deposition rate with respect to other AM technologies. Despite these great benefits, WAAM components are affected by severe distortions and residual stresses issues. Finite element process simulation provides an efficient way to study mitigation strategies for such issues. In this paper, a WAAM modelling strategy is proposed based on a novel heat source model that takes into account the actual power distribution between filler and base materials. In order to prove the effectiveness of proposed modelling, an experimental validation is provided by comparing the measured distortions of a WAAM tests-case with the simulated ones, highlighting the accuracy of proposed model.

Peer-review under responsibility of the scientific committee of the 5th CIRP Global Web Conference Research and Innovation for Future Production

Keywords: Welding; Finite element method (FEM); Additive manufacturing;

1. Introduction

Additive Manufacturing (AM) processes, for the production of metal components, represent one of the most relevant innovations in the manufacturing sector. Indeed, such technologies provide several benefits such as the possibility of manufacturing parts with complex geometries and a significant reduction of material waste with respect to machining processes. Among metal AM processes, Wire-Arc-Additive-Manufacturing (WAAM) is one of the most efficient in terms of deposition rate (2÷10 [kg/h]) [1] and allows to manufacture large components, up to several meters [2]. In this process, the part is created stacking subsequent layers by means of an arc welding process, generally Gas-Metal-Arc-Welding (GMAW).

Despite WAAM advantages, components manufactured with such technology are prone to residual stresses and distortions issues [3] affecting the subsequent machining operations [4]. The cause of such phenomena is the non-uniform temperature field experienced by the component during the deposition process, strictly connected to the deposition path [5]. Process simulation is a powerful tool to tackle such issues, allowing to test the effect of different deposition patterns on residual stresses field, optimizing the process[6]. Furthermore, post-process machining operations can be simulated, assessing their effects on AM parts distortions and residual stresses([7],[8]).

From a simulation perspective, WAAM process is very similar to multi-pass welding process. The heat and mass transfer between the arc and the workpiece is governed by the molten pool, characterized by complex physical phenomena. Despite some works focus on molten pool and arc dynamics simulation [9], it is not possible to apply such complex techniques at component scale level, due to the unacceptable computational time requirements. Therefore, the process is usually simulated by means of coupled thermo-mechanical Finite-Element (FE) analyses. Basically, the heat transfer from the arc to the molten pool is simulated using a heat source model, which prescribes a heat generation per unit volume in the molten pool region. Material deposition is taken into account by means of specific elements activation algorithms [10]. Many researchers focused on improving simulation accuracy and efficiency: J.Ding et al. [11] developed a steady state approach tailored for the simulation of large parts

Peer-review under responsibility of the scientific committee of the 5th CIRP Global Web Conference Research and Innovation for Future Production
doi:10.1016/j.procir.2016.08.024

manufacturing; Bai et al. [12] proposed an infra-red imaging procedure to calibrate model input parameter; Michaleris [13] compared material deposition modelling techniques and proposed an algorithm to improve its accuracy and efficiency.

In most of literature works dealing with AM simulation, the heat source model proposed by Goldak et al. [14] is used. In this model the heat input is delivered over a moving double ellipsoid region according to a Gaussian distribution. Despite such strategy permits to correctly model the shape of the weld pool, it does not take into account the correct heat distribution between filler and base material. This is responsible for inaccuracies in part distortions estimation.

In this paper, the WAAM process is simulated using a novel definition of the heat source, based on a modified Goldak model, in order to have a more realistic heat flow distribution in the filler material. In the following sections, Goldak model is discussed highlighting its criticalities. Proposed simulation technique and heat source model are then presented. Finally the measured distortion of a test case component, manufactured by means of WAAM process, are compared with FE results obtained with the proposed and the Goldak heat source models.

Nomenclature

$a_{f,r}$	Ellipsoid x semi axis (front or rear)
b	Ellipsoid y semi axis
c	Ellipsoid z semi axis (front)
C_p^{eq}	Equivalent heat capacity
d_{el}	Bead finite elements length in feed direction
$f_{f,r}$	Ellipsoid distribution factor (front and rear)
h_l	Bead model height
h_{lat}	Latent heat of fusion
i	Welding current
l	Filler metal heat source length in feed direction
$P(T)$	Generic material property
P_{act}	Material property in active state
P_{quiet}	Material property in quiet state
$\dot{q}_v$	Goldak power density function
$\dot{q}_b$	Base material power density function
$\dot{q}_w$	Filler material power density function
q_w	Energy density transmitted to filler metal segment
q_{eq}	Equivalent power density function
$\dot{Q}_b$	Thermal power transmitted to the base material
$\dot{Q}_w$	Thermal power transmitted to the filler material
T	Temperature
T_{sol}	Solid temperature
T_{liq}	Liquid temperature
V	Welding voltage
v_f	Feed speed
V_{el}	Bead finite elements length in feed direction
$\dot{V}$	Material volume flow rate
w_l	Bead model width
η	Heat source efficiency
ρ	Material mass density
τ	Filler metal model heating time

2. Double ellipsoid heat source model

The Goldak model prescribes a Gaussian distributed heat generation per unit volume defined in a moving frame of reference, shown in Figure 1: *x* axis is oriented in the feed direction, *z* axis in the arc aiming direction and *y* is defined according to the right hand rule.

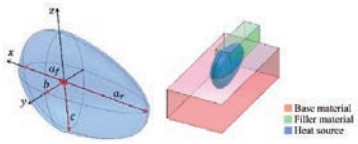

Figure 1: Goldak double ellipsoid model

Basically two different power distribution functions are defined for positive and negative x semi axes, allowing to model asymmetries in heat distribution over the molten pool. Eq. 1 shows the power density distribution functions:

$$\dot{q}_v = \frac{6\sqrt{3}\dot{Q}f_{f,r}}{\pi\sqrt{\pi}a_{f,r}bc}\exp\left[-3\left(\frac{x^2}{a_{f,r}^2}+\frac{y^2}{b^2}+\frac{z^2}{c^2}\right)\right] \quad (1)$$

Coefficients $a_{f,r}$, b and c are the semi axes of two ellipsoids centered in the origin of the frame of reference, as shown in Figure 1. The double subscript for the parameter a means that different values are used depending on x sign (a_f if positive and a_r if negative) leading to two different functions. Ellipsoid surface represent the space region where the power density falls to 5% of its peak value. Usually the value of ellipsoids semi axes is set according to molten pool dimension [15]. The terms $f_{f,r}$ are the distribution factors, having different values for the frontward and backward ellipsoids, provided that the following condition is fulfilled [14]:

$$f_f + f_r = 2 \quad (2)$$

$\dot{Q}$ is the heat input per unit time and it is computed as the product of welding current, welding voltage and arc efficiency, as described by eq. (3):

$$\dot{Q} = \eta i V \quad (3)$$

Integrating the two power density functions in spatial coordinates returns the total energy input per unit time generated by the heat source. According to Goldak this integration returns the following result [14]:

$$\int_{-\infty}^{+\infty}\int_{-\infty}^{+\infty}\int_{-\infty}^{+\infty}\dot{q}_V(x,y,z)dxdydz = 2\dot{Q} \quad (4)$$

According to this model, the actual power transmitted to the workpiece depends on the relative position between the heat source frame of reference and the base material. If such origin is positioned on the top surface of the base material, as shown in Figure 1, the heat input is transmitted both to the base and filler material. According to eq. 4 transmitted power will be higher than the actual process heat input $\dot{Q}$. This might lead to severe overshoots in molten pool temperature. On the contrary, positioning the origin on the top the filler material would be correct for what concerns the transmitted power, but most of the heat will be delivered to the filler metal, resulting in a poor weld penetration. This issue could be overcome modifying ellipsoids semi axes values, resulting in a time consuming model updating procedure that could lead to values without physical meaning. Therefore, adopting a heat source model that takes into account the actual power subdivision between filler and base metal would both improve modelling accuracy and simplify model parameter set up phase.

3. Proposed model

In this section proposed WAAM modeling technique will be presented. First, the heat source model will be described in section 3.1. Section 3.2 will be focused on the elements activation algorithm.

3.1. Heat source model

As earlier mentioned, Goldak model does not allow to take into account the actual power distribution between filler and base metal. Indeed, in GMAW, there are two ways in which arc power is transferred to the molten pool: direct transfer from electric arc to the base metal and filler metal melting energy transferred by means of droplets enthalpy. According to previous works [16], the power consumed in melting filler metal is about 50% of total arc power. Therefore, an accurate heat source model should take such power distribution into account.

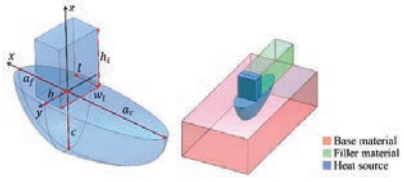

Figure 2: Proposed heat source model.

The base concept is to adopt different power distributions for the filler and base material: part of the total power is delivered to the base material by a Goldak Gaussian distribution, while the remaining one is distributed over the filler material with a constant pattern. This allows to capture the steep temperature gradients in the molten pool, accurately described by Goldak heat source [17] and transmit the correct amount of heat to the filler material elements. Figure 2 shows the heat source positioning with respect to the substrate, while proposed power density function is presented in eq. (5).

$$\begin{cases} \dot{q}_b = \dfrac{6\sqrt{3}\dot{Q}_b f_{f,r}}{\pi\sqrt{\pi}a_{f,r}bc}\exp\left[-3\left(\dfrac{x^2}{a_{f,r}^2}+\dfrac{y^2}{b^2}+\dfrac{z^2}{c^2}\right)\right] \\ \dot{q}_w = \dfrac{\dot{Q}_w}{Vel} \end{cases} \quad (5)$$

Subscripts f and r have been assigned according to the notation presented in section2. $\dot{Q}_w$ and $\dot{Q}_b$ are the total powers delivered respectively to the filler and the base metal. Since, according to literature, the amount of total power consumed in melting filler material is roughly 50% [16], as first approximation $\dot{Q}_w$ and $\dot{Q}_b$ can be set as shown in eq. (6):

$$\dot{Q}_w = \dot{Q}_b = \frac{\eta i V}{2} \quad (6)$$

As earlier mentioned, the power transmitted to the substrate is taken into account according to Goldak double ellipsoid model, while for the filler metal a specific model was developed. Basically an internal heat generation is applied to the filler FE elements whose centroid lies inside a brick shaped control volume, moving according to deposition path, as shown Figure 2. The power density value is defined as the ratio between the wire melting power and the volume of the elements currently heated by the power source. Such volume depends on the heat source size along feed direction, l defined in Figure 2. The value of such parameter must be defined in order to transmit the correct amount of energy to filler FE elements. As first approximation the weld bead can be modelled with a rectangular cross section, using hexahedral elements with a drag pattern along the feed direction as shown in Figure 3.

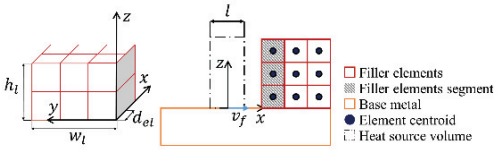

Figure 3: Filler mesh interaction with proposed heat source model.

Let d_{el} be the size of filler FE elements along the feed direction. In proposed model the control volume cross section has the same dimensions of the weld bead, i.e w_l and h_l, as outlined in Figure 2. The heat transmitted to the filler material per unit volume can be computed as the ratio between filler power and material flow rate:

$$q_w = \frac{\dot{Q}_w}{\dot{V}} = \frac{\dot{Q}_w}{v_f w_l h_l} \quad (7)$$

Where v_f represents the feed speed of the welding head. This value should be equal to the energy per unit volume actually

transmitted to the workpiece in the FE model. If power density function is kept constant throughout the element volume V_{el}, the energy per unit volume transmitted to filler in the FE model can be computed according to eq. (8):

$$q_w = \frac{\dot{Q}_w}{V_{el}}\tau = \frac{\dot{Q}_w}{w_l h_l d_{el}}\frac{l}{v_f} \tag{8}$$

Where τ is the time interval in which the centroids of the FE elements corresponding to a single segment, lies inside the control volume. Since the expressions of q_w given by eq. 7 and 8 must be equivalent, the heat source length to be finally identified:

$$l = d_{el} \tag{9}$$

Therefore, heat source dimension in feed direction must be equal to the correspondent size of filler FE elements, in order to transmit them the correct amount of energy. In summary, proposed heat source model allows to transmit the correct amount of thermal power to the FE model, taking into account the actual subdivision of the energy between filler and base material.

3.2. Deposition modeling

AM simulation requires specific elements activation techniques to simulate material deposition. Two main groups of approaches exist: inactive element method and quiet element method [18]. In this work a quiet element method technique borrowed from welding simulation [19] is used. In quiet element methods, filler metal elements are present throughout all the simulation but initially quiet values are assigned to their thermal and elastic properties (e.g. low Young's modulus and thermal conductivity) in order to minimize their influence on the component behavior. Material properties are progressively switched from quiet to active values according to the deposition process, simulating material deposition. In the adopted approach, elements switch from quiet to active state is triggered by temperature. The basic principle is that quiet material has an extremely low thermal conductivity hence filler elements in quiet state will experience a significant increase in temperature only if they are directly heated by the external power source. To implement this technique material properties values are computed according to eq. 10:

$$P(T) = \gamma(T_{\max})P_{act}(T) + (1-\gamma(T))P_{quiet} \tag{10}$$

Where P_{act} and P_{quiet} represent the generic material property in active and quiet state respectively, γ is the activation function depending on T_{max} that is the maximum temperature experienced by the element from the start to the current simulation time. Activation function pattern is shown in Figure 4. It it is highlighted that the transition from quiet to active state occurs within a temperature range, rather than at a specific temperature value, in order to avoid simulation convergence issues.

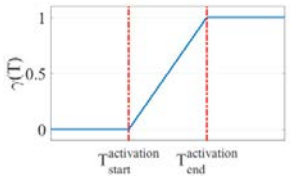

Figure 4: Elements activation function.

In this work activation start and end temperature are set according to material liquidus and solidus temperatures respectively.

Another important issue to be cared for is the latent heat implementation. Indeed in the phase transition range, material thermal inertia results to be significantly higher with respect to the solid and liquid state. This is particularly important with proposed activation strategies, where elements temperature controls the quiet to active transition. The most common approach to treat latent heat is to raise artificially material heat capacity in the phase transition range [20], imposing the equivalence between enthalpy variation and latent heat. In this approach, an excessive increase of the heat capacity could lead to simulation convergence issues. To overcome this issue, it is proposed to take latent heat into account prescribing a power generation per unit volume proportional to temperature time derivative as stated in eq. 11:

$$\begin{cases} T_{sol} > T > T_{liq} \quad \dot{q}_{eq}=0 \\ T_{sol} \le T \le T_{liq} \quad \dot{q}_{eq} = -\dfrac{dT}{dt}\left(\dfrac{\rho h_{lat}}{T_{liq}-T_{sol}}\right) \end{cases} \tag{11}$$

It must be pointed out that if material is melting the generated heat is negative i.e. it is subtracted from material internal energy. On the contrary, during material solidification the generated heat will be positive, hence added to material internal energy. If power generation function is integrated over the phase transition temperature range, the total amount of heat generated per unit volume will be equivalent to the latent heat of fusion. Hence prescribed heat generation function allows latent heat effect to be taken into account without causing convergence issues.

4. Model validation

The accuracy of proposed model was tested analyzing the correlation of simulated and actual distortions, in two different test cases: a simple welding bead and a wall, i.e. five straight layers stacked on to each other. Manufacturing of both samples was carried out by WAAM technique using a prototype machine assembled in our laboratory. Figure 5 shows test cases dimensions. Both bead on plate and wall had the same length and were deposed onto a base plate having the same dimensions. Components distortions in Z direction (shown in Figure 5) were measured by means of a Coordinate-Measurement-Machine (CMM), and experimental results were then compared with FE model results.

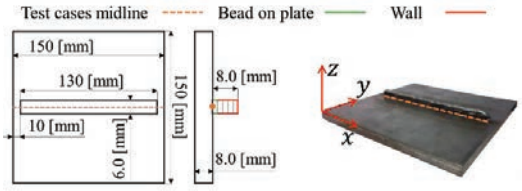

Figure 5: Test cases dimension and actual wall test case

In order to compare proposed modelling strategy with the traditional Goldak heat source model the single bead test case was FE modelled using both techniques. In section 4.1, experimental tests execution and manufacturing procedures will be discussed. In section 4.2 the details concerning test case FE model will be provided, while results will be presented and discussed in section 4.3.

4.1. Experimental tests

Proposed test cases base plate material was S235JR structural steel while the beads were manufactured using an ER70S-6 metal wire with 0.8 mm diameter. Deposition was carried out using a Millermatic 300 direct current GMAW welding unit, using the following process parameters: travelling speed 300 mm/min, wire feed speed 4.6 m/min, open circuit voltage 19 V, average welding current 81 A, average welding voltage 18.1 V. Welding current and voltage were measured during the manufacturing process, in order to accurately quantify the average thermal power value to be used in the heat source model. (1480 W). In wall manufacturing, layers were deposed with an interpass dwell period of 10 s. Workpieces fixture adopted an isostatic solution in order to eliminate the influence of the unclamping phase on components final distortions. This was achieved placing the base plate onto a three points support.

Components top surface was scanned with a Mitutoyo Euro Apex C776 CMM. Specimen were scanned before and after the WAAM operation, in order to evaluate the Z component of the displacement field, with respect to the frame of reference shown in Figure 5. This process allowed to evaluate the correlation between experiments and model results, excluding the influence of top surface unevenness.

4.2. Test case modelling

The FE model of the test case described in previous section was created using the developed techniques. Analyses were carried out using LS-Dyna commercial finite element code. The overall geometry, including both filler and base metal, was discretized using 37800, 8-nodes brick elements. Test case FE model is presented in Figure 6. Manufacturing process simulation was carried out using a coupled transient thermo-mechanical solution routine. Such simulation was carried out using a Crank-Nicholson integration scheme for the heat transfer solution and a fully implicit one for the mechanics equations.

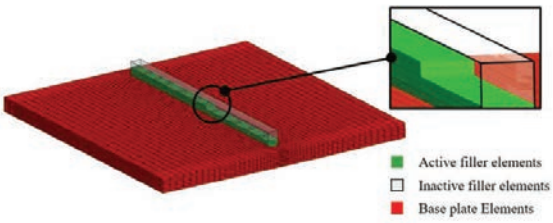

Figure 6: FE model of the test case.

Heat source was modelled according to the proposed technique. Heat source parameters used in test case manufacturing simulation are summarized in Table 1: ellipsoid parameters were set according to molten pool dimension, while the length of the filler metal heat source were set consistently with proposed procedure.

Table 1: Heat source parameters.

a_f [mm]	a_r [mm]	b [mm]	c [mm]	f_f [mm]	f_r [mm]	l [mm]
1.4	3.5	3.0	3.0	0.6	1.4	1.4

Material properties were assumed to be temperature dependent and their values were obtained from technical literature [21]. Material mechanical behavior was modelled neglecting strain and rate hardening effects, while thermal softening was taken into account considering the yield stress to be temperature dependent.

Free convection boundary conditions were set up on the base plate top and bottom surfaces and on the wall vertical surfaces. Convection coefficients values, set according to literature correlations [21], were: 8.5 [W/m^{2}K] for the base plate top surface, 4.0 [W/m^{2}K] for the bottom surface and 12.0 [W/m^{2}K] for the wall vertical surface. A boundary condition of general radiation to environment was included, setting material emissivity was set to 0.2. Environment and material initial temperatures were set to 298.16 [K]. Mechanical boundary conditions were included in the model by means of single point constrains.

4.3. Results and discussion

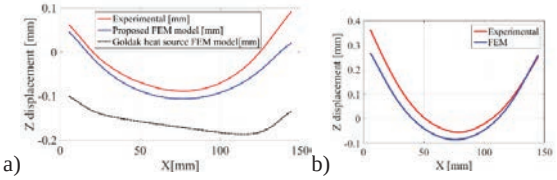

Figure 7: Midline displacements for the bead on plate (a) and the wall test cases (b).

FEM and experimental midline displacements have been compared for the both the test cases. As shown in Figure 5 for the wall and bead on plate test cases the mean line is defined as the weld bead axis in correspondence of the base plate, hence at z coordinate 0 value. Figure 7a shows bead on plate test results, while Figure 7b shows the ones related to the wall test.

From bead on plate test outcomes it is clear that Goldak model leads to a remarkable overshoot in midline displacement. On the other hand, proposed model allows to achieve a good correlation between simulated and measured displacement field. This result could be explained comparing temperature distributions of the two modelling strategies, shown in Figure . It is clear that Goldak model (Figure 8a) leads to an higher temperature peak in the molten region (orange and red colors) than proposed modelling strategy (Figure 8b). This is due to the larger amount of heat delivered by the Goldak heat source in opposition to proposed model that transmits the correct amount of heat to the FE model, hence resulting in a lower peak temperature. This could explain the different correlation of FE models displacements with the experimental data.

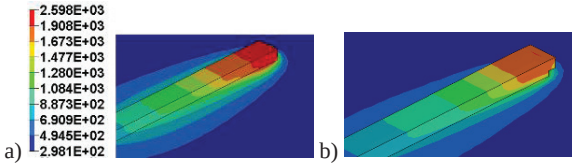

Figure 8: Bead on plate models temperature field a) Goldak b)Proposed model

This is consistent with the results obtained in the wall test case (**Errore. L'origine riferimento non è stata trovata.**). It can be noticed that, despite some discrepancies proposed model results are in good agreement with the experimental one. Percentage errors on the maximum displacements points are 2% and 26%. Despite the latter result may seem inaccurate, it should be considered that material data have been derived from literature, hence actual material behavior could be different from the model one. Furthermore, no tuning operation was carried out for what concerns convection coefficients and heat source parameters, as it is usually performed in works dealing with WAAM simulation. Hence proposed model returns a reliable prediction of displacement field general pattern with a good punctual accuracy, that can be improved with a better representation of actual material behavior and boundary conditions.

5. Conclusions

In this work a WAAM modelling technique is proposed. A novel heat source model is developed, which allows to take into account the actual power distribution between base and filler material. Element activation strategy is presented and an alternative way to include latent heat of fusion effects without causing convergence issues is developed. Proposed process modelling was validated and compared with traditional heat source modelling. Experimentally measured distortions of two test cases, were compared with the ones predicted by proposed FEM simulation and Goldak modelling. Validation procedure highlighted that despite some inaccuracies, proposed modelling results are in general agreement with the experimental ones, allowing to achieve an higher accuracy with respect to the traditional technique. Hence, proposed process modelling allows to accurately simulate the WAAM process, without the need to perform time-consuming tuning operations to identify heat source parameters.

References

[1] Ding D, Pan Z, Cuiuri D, Li H. Wire-feed additive manufacturing of metal components: technologies, developments and future interests. Int J Adv Manuf Technol 2015;81:465–81.
[2] Ding D, Pan Z, Cuiuri D, Li H. A multi-bead overlapping model for robotic wire and arc additive manufacturing (WAAM). Robot Comput Integr Manuf 2015;31:101–10.
[3] Szost BA, Terzi S, Martina F, Boisselier D, Prytuliak A, Pirling T, Hofmann M, Jarvis DJ. A comparative study of additive manufacturing techniques: Residual stress and microstructural analysis of CLAD and WAAM printed Ti-6Al-4V components. Mater Des 2016;89:559–67.
[4] Montevecchi F, Grossi N, Takagi H, Scippa A, Sasahara H, Campatelli G. Cutting forces analysis in additive manufactured AISI H13 alloy. Procedia CIRP 2016.
[5] Colegrove PA, Coules HE, Fairman J, Martina F, Kashoob T, Mamash H, Cozzolino LD. Microstructure and residual stress improvement in wire and arc additively manufactured parts through high-pressure rolling. J Mater Process Technol 2013;213:1782–91.
[6] Schoinochoritis B, Chantzis D, Salonitis K. Simulation of metallic powder bed additive manufacturing processes with the finite element method: A critical review. Proc Inst Mech Eng Part B J Eng Manuf 2015.
[7] Salonitis K, D'Alvise L, Schoinochoritis B, Chantzis D. Additive manufacturing and post-processing simulation: laser cladding followed by high speed machining. Int J Adv Manuf Technol 2015:1–11.
[8] D'Alvise L, Chantzis D, Schoinochoritis B, Salonitis K. Modelling of Part Distortion Due to Residual Stresses Relaxation: An aerOnautical Case Study. Procedia CIRP 2015;31:447–52.
[9] Hu J, Tsai HL. Heat and mass transfer in gas metal arc welding. Part I: The arc. Int J Heat Mass Transf 2007;50:833–46.
[10] Martukanitz R, Michaleris P, Palmer T, DebRoy T, Liu ZK, Otis R, Heo TW, Chen LQ. Toward an integrated computational system for describing the additive manufacturing process for metallic materials. Addit Manuf 2014;1:52–63.
[11] Ding J, Colegrove P, Mehnen J, Ganguly S, Almeida PMS, Wang F, Williams S. Thermo-mechanical analysis of Wire and Arc Additive Layer Manufacturing process on large multi-layer parts. Comput Mater Sci 2011;50:3315–22.
[12] Bai X, Zhang H, Wang G. Improving prediction accuracy of thermal analysis for weld-based additive manufacturing by calibrating input parameters using IR imaging. Int J Adv Manuf Technol 2013;69:1087–95.
[13] Michaleris P. Modeling metal deposition in heat transfer analyses of additive manufacturing processes. Finite Elem Anal Des 2014;86:51–60.
[14] Goldak J, Chakravarti A, Bibby M. A new finite element model for welding heat sources. Metall Trans B 1984;15:299–305.
[15] Hao M, Sun Y. A FEM model for simulating temperature field in coaxial laser cladding of TI6AL4V alloy using an inverse modeling approach. Int J Heat Mass Transf 2013;64:352–60.
[16] Dupont JN, Marder AR. Thermal Efficiency of Arc Welding Processes. Weld Res Suppl 1995:406s – 416s.
[17] Goldak J, Bibby M, Moore J, House R, Patel B. Computer modeling of heat flow in welds. Metall Trans B 1986;17:\textsc{587–600}.
[18] Chiumenti M, Cervera M, Salmi A, Agelet de Saracibar C, Dialami N, Matsui K. Finite element modeling of multi-pass welding and shaped metal deposition processes. Comput Methods Appl Mech Eng 2010;199:2343–59.
[19] Lindström P, Josefson B, Schill M, Borrvall T. Constitutive Modeling and Finite Element Simulation of Multi Pass Girth Welds. Proc. NAFEMS Nord. Conf., Gothernburg: 2012, p. 22–3.
[20] Hussein A, Hao L, Yan C, Everson R. Finite element simulation of the temperature and stress fields in single layers built without-support in selective laser melting. Mater Des 2013;52:638–47.
[21] EPRI. Carbon Steel Handbook. vol. 3. Palo Alto (CA): 2007.